

Vibrationally Assisted Direct Intersystem Crossing between the Same Charge-Transfer States for Thermally Activated Delayed Fluorescence: Analysis by Marcus–Hush Theory Including Reorganization Energy

Illia E. Serdiuk,* Michał Mońka, Karol Kozakiewicz, Beata Liberek, Piotr Bojarski, and Soo Young Park



Cite This: *J. Phys. Chem. B* 2021, 125, 2696–2706



Read Online

ACCESS |



Metrics & More

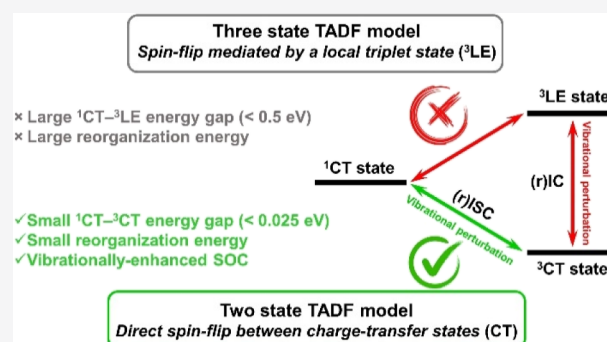


Article Recommendations



Supporting Information

ABSTRACT: Thermally activated delayed fluorescence (TADF) has recently become an extensively investigated phenomenon due to its high potential for application in organic optoelectronics. Currently, there is still lack of a model describing correctly basic photophysical parameters of organic TADF emitters. This article presents such a photophysical model describing the rates of intersystem crossing (ISC), reverse ISC (rISC), and radiative deactivation in various media and emphasizing key importance of molecular vibrations on the example of a popular TADF dye 9,10-dihydro-9,9-dimethyl-10-(4-(4,6-diphenyl-1,3,5-triazin-2-yl)phenyl)-acridine (DMAC-TRZ). The presented experimental and theoretical investigations prove that ISC and rISC can occur efficiently between the singlet and triplet states of the same charge-transfer nature (^1CT and ^3CT , respectively). In emitters with the orthogonal donor and acceptor fragments, such spin-forbidden $^1\text{CT} \leftrightarrow ^3\text{CT}$ transitions are activated by molecular vibrations. Namely, the change of dihedral angle between the donor and the acceptor affords reasonable spin–orbit coupling, which together with a small energy gap and reorganization energy enable $^1\text{CT} \leftrightarrow ^3\text{CT}$ transition rates reaching $1 \times 10^7 \text{ s}^{-1}$. Evidence of direct $^1\text{CT} \leftrightarrow ^3\text{CT}$ spin-flip and negligible role of a second triplet state, widely believed as a key parameter in the design of (r)ISC materials, change significantly the current understanding of TADF mechanism. In authors' opinion, photophysics, and molecular design principles of TADF emitters should be revised considering the importance of vibrationally enhanced $^1\text{CT} \leftrightarrow ^3\text{CT}$ transitions.



INTRODUCTION

Over the last decade, fast development of all-organic optoelectronics with an increasing number of potential applications provided a plethora of experimental solutions on the (sub)molecular level. In one of the most promising applications of all-organic light-emitting diodes (OLEDs), these solutions are mainly focused on the problem of triplet harvesting. Due to spin statistics, recombination of charges in organic semiconductors leads to formation of singlet (25%) and triplet (75%) excitons. In heavy-atom free molecular systems, triplet excitons usually cannot ensure fast rates of light emission and should be converted to the singlet ones for high electroluminescence efficiency.

Currently, probably the best solution for triplet harvesting is the use of materials with fast reverse intersystem crossing (rISC). This can be realized either by emitters exhibiting thermally activated delayed fluorescence (TADF) dispersed in common OLED hosts¹ or by common fluorescent emitters dispersed in TADF emitters in the role of hosts, the so-called “hyperfluorescence” approach.² Numerous photo- and electro-luminescent investigations revealed strong dependence of

internal and external quantum efficiencies on the rISC rate. The importance of materials with fast rISC for further development of optoelectronics cannot be thus overestimated.

Up to the moment, there has been no general theoretical model which would correctly describe the basic photophysical parameters of TADF materials such as rates of intersystem crossing (ISC), rISC, and radiative deactivation in various media. Obviously, this impedes correct understanding of the mechanism and design principles of efficient TADF materials. In this article, we present such a model and on the example of one of the most popular TADF emitters explain how high rISC and ISC rates are achieved under various conditions. To date, all organic emitters with superior rISC rates are built of spatially separated strong electronic donor and acceptor

Received: November 25, 2020

Revised: January 31, 2021

Published: March 4, 2021



molecular fragments, which is the key principle of design strategy of TADF emitters. Such a structure enables formation of charge-transfer (CT) states, which represent the lowest excited singlet ^1CT and triplet ^3CT electronic states. Efficient separation of the donor and acceptor provides a negligible overlap of highest occupied molecular orbital (HOMO) and lowest unoccupied molecular orbital (LUMO), which decreases the exchange and energy gap ($\Delta E_{\text{CT}-^3\text{CT}}$) between the ^1CT and ^3CT states. All theoretical models developed before to describe the bases of TADF photophysics follow the selection rule stating that spin-flip between the ^1CT and ^3CT states is forbidden due to their identical nature. In fact, state-of-the-art methods of quantum chemistry predict a zero spin-orbit coupling constant (SOCME) for the ^1CT and ^3CT interaction. For this reason, TADF efficiency is believed to be strongly dependent on the presence of at least one additional triplet state with close energy to the ^1CT and ^3CT ones. This can be either a locally excited ^3LE state localized on a donor or an acceptor³ or another CT state formed via electronic transition on different molecular orbitals.⁴ According to this, rISC is mediated by this third state because the transition between it and the ^1CT state is more allowed due to their different nature. The presence of such a third state is believed as another key requirement in the design of TADF emitters.

Among the above-described cases, the one relying on the energetically close donor or acceptor ^3LE state has been used to explain the majority of TADF examples including a triazine derivative 9,10-dihydro-9,9-dimethyl-10-(4-(4,6-diphenyl-1,3,5-triazin-2-yl)phenyl)-acridine (DMAC-TRZ) investigated here. It should be emphasized that such a three-state model predicts maximum rISC rate when ^3LE and $^3\text{CT}/^1\text{CT}$ states are energetically close. In terms of spectroscopic parameters measured experimentally, this means that the energy gap between ^1CT and ^3LE states ($\Delta E_{\text{CT}-^3\text{LE}}$) should be zero. More advanced variations of the three-state model specify an additional condition for maximal rISC: vibronic coupling between ^3LE and ^3CT states.⁵ Similar criterion is found in another theoretical model, which assumes that the T_1 state of various *s*-triazine and benzonitrile emitters is not of pure CT-nature but contains various portions of LE nature.⁶ Such a model thus suggests different nature of S_1 and T_1 states, which provides relatively high SOCME values and in such a way explains efficient rISC. The extent of LE contribution can be substantial in a non-polar medium, when CT energy is close to the triplet energy of a separate acceptor or donor, but it should decrease when CT is stabilized in high-polarity media. As follows from all these models, when the lowest CT states are stabilized and the $\Delta E_{\text{CT}-^3\text{LE}}$ energy gap increases by module, the rISC rate should decrease sharply. What is more, the same conclusion should be true for the forward ISC transition because it should also strongly depend on $\Delta E_{\text{CT}-^3\text{LE}}$. Here, we provide evidence that such conclusions on the dependence of ISC and rISC rates on the $\Delta E_{\text{CT}-^3\text{LE}}$ value are not supported by the experiment.

Some previous articles have already pointed at some discrepancies between the three-state model and the experimental behavior of TADF emitters. Namely, some of the investigations evidence the key role of molecular vibrations in TADF photophysics. For example, introduction of methyl groups at positions 1 and/or 9 of phenothiazine donor decreases drastically TADF rate and efficiency of phenothiazine-dibenzothiothiophene-*S,S*-dioxide emitters even in liquid solutions.⁷ In this case, in spite of low $\Delta E_{\text{CT}-^3\text{LE}}$ value, the

restriction of some undetermined molecular vibrations by methyl groups was concluded to be extremely important for rISC: the more the vibrational freedom was restricted, the less TADF efficiency was observed. In the case of less flexible derivatives with more bulky isopropyl or *tert*-butyl groups, TADF was almost absent and the T_1 state deactivated mainly via room-temperature phosphorescence. Next, it was found that the explanation of the radiative rate of TADF emitters with orthogonal donor and acceptor fragments is not possible within “frozen” optimized geometry because of zero oscillator strength predicted by calculations.⁸ It was proved that molecular vibrations should be taken into account for adequate prediction of oscillator strength and electronic transition moment. In another recent investigation, the behavior of DMAC-TRZ in solid solutions was explained by the inhomogeneity of its geometry caused by rotational isomerism and distribution of CT states.⁹ Another recent theoretical model assumed that both spin-orbit coupling (SOC, $T_2/T_1 \rightarrow S_1$) and the so-called direct SOC ($T_1 \rightarrow S_1$) play important roles in rISC.¹⁰ However, the direct $T_1 \rightarrow S_1$ transition was predicted to be efficient when the nature of T_1 and S_1 states is different: the presented calculations predicted 92% CT nature for the S_1 state and 95% LE nature for the T_1 state. The proposed model can thus also be valid only in the case of the proximity of ^1CT and ^3LE states. Despite the fact that the above-mentioned investigations were still explained by the three-state model, these experimental results question the primary importance of minimal $\Delta E_{\text{CT}-^3\text{LE}}$ value for a maximum rISC rate at $T > 0$ K where molecules exist in various excited vibronic states.

The importance of molecular vibrations for efficient TADF was also suggested for the carbene-heavy-metal complexes.¹¹ Fast rISC in such emitters was explained by the thermally activated rotation along the bond between the metal atom and the donor fragment, which decreased the $\Delta E_{\text{CT}-^3\text{CT}}$ value and facilitated direct $T_1 \rightarrow S_1$ transition. Together with the reasonable SOC values¹² due to heavy-atom effect, this resulted in high TADF rate constant (ca. $3 \times 10^6 \text{ s}^{-1}$). Further investigations of similar compounds revealed that the energetic closeness of ^3LE state itself does not reduce the activation energy of rISC but results in the undesired decrease of emissive rate of the S_1-S_0 transition.¹³

It should also be noticed that according to the three-state model, the differences between the ^1CT and ^3LE states should favor the interaction between them. However, different electronic structures lead to the differences in geometry. In terms of Marcus semiclassical electron-transfer theory,⁶ this means the increase of reorganization energy of $^1\text{CT} \leftrightarrow ^3\text{LE}$ transitions ($\lambda_{\text{CT} \leftrightarrow ^3\text{LE}}$) and should not increase but rather decrease their rates. The investigations presented here prove that minimization of reorganization energy is as much important as small energy gap between singlet and triplet state (ΔE_{ST}) value for achieving high rates of ISC and rISC. Substantial differences in the reorganization energies play the decisive role in favor of $^3\text{CT} \leftrightarrow ^1\text{CT}$ transitions but not the $^1\text{CT} \leftrightarrow ^3\text{LE}$ ones.

In this research, to check the widely accepted importance of ^3LE state for spin-flip transitions, both $\Delta E_{\text{CT}-^3\text{CT}}$ and $\Delta E_{\text{CT}-^3\text{LE}}$ values were scanned experimentally. One of the most simple and basic but reliable spectroscopic experiments was conducted—solvatochromic measurements. The use of media of different polarities provides information on the effect of alignment of energy levels on all basic photophysical

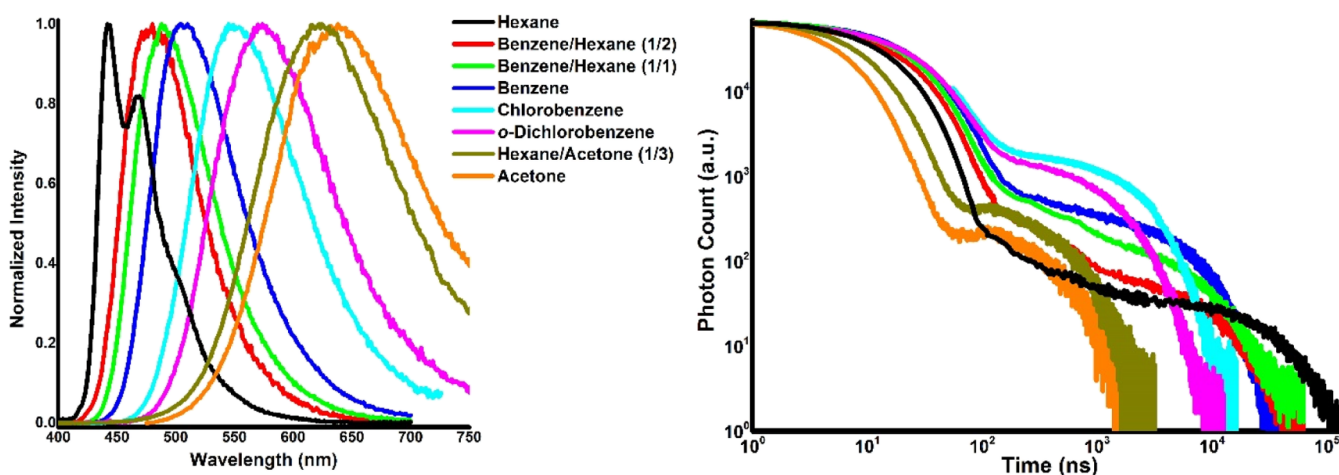


Figure 1. Intensity-normalized emission spectra and decays of DMAC-TRZ in various solutions.

parameters, which is especially valuable for understanding TADF photophysics. DMAC-TRZ emitter was selected, which together with its various derivatives exhibits one of the best photo- and electroluminescent characteristics extensively studied lately.^{14,15} Due to the high transition dipole moment of the ¹CT and ³CT states, their energies were effectively decreased with increasing medium polarity. Localized transitions are much less sensitive to the polarity of medium; therefore, the ³LE value is concerned as a constant. Thus, manipulation of solvent polarity, in a common notion meaning overall solvation capability, allowed us to tune ΔE_{CT-LE} from positive (low polarity, $E_{CT} > E_{LE}$) to negative (higher polarity, $E_{CT} < E_{LE}$) values. Importantly, evidence was found that the energy gap between ¹CT and ³CT states also changes with polarity. In spite of experimental simplicity of solvatochromic experiment, it remains a challenging task for calculations using the methods of time-dependent density functional theory (TDDFT). For this reason, the results of calculations were treated here with special attention and analyzed only in the case of good correlation with experimental data.

METHODS

DMAC-TRZ was synthesized as reported previously¹⁶ and purified by sublimation in vacuum. Solvents for photophysical measurements were of spectroscopic grade or higher. All the photophysical measurements were conducted in the argon atmosphere.

Steady-state photoluminescence spectra were obtained with a PTI QuantaMaster 40 spectrofluorometer. All the emission spectra were corrected on the photodetector sensitivity. Photoluminescence quantum yields (PLQY) were obtained using 9,10-diphenylanthracene in cyclohexane (93%) as a reference.¹⁷ Time-dependent emission measurements at room temperature were obtained using a FluoTime 300 fluorescence lifetime spectrometer equipped with a LDH-P-C-375 laser head. The parameters of photophysical processes were calculated using equations described in the literature;^{18,19} for details, see the Supporting Information.

Quantum-Chemical Calculations. The unconstrained geometry optimizations of DMAC-TRZ were performed for the ground (S_0), excited singlet (S_1), and triplet (T_1 , T_2 , and T_3) electronic states at DFT/TDDFT level of theory²⁰ using the Gaussian 16 program package.²¹ The B3LYP²² hybrid functional was used with the cc-pVDZ basis set. Nature of

states (CT or LE) was established on the basis of analysis of molecular orbitals involved in each transition, for details, see the Supporting Information, Scheme S1. The energies of ¹CT- S_0 , ¹CT-³CT, and ¹CT-³LE transitions were obtained by single-point calculations using the optimized geometry of ¹CT state (S_1); the respective values for the ³CT- S_0 , ³CT-¹CT and ³LE- S_0 , ³LE-¹CT transitions were obtained by single-point calculations using the optimized geometries of ³CT (T_1) and ³LE (T_2), respectively. Computational ΔE_{CT-3CT} and ΔE_{CT-3LE} values represent differences between minimal energies of respective states. The electronic energies and transition energies of rotational isomers in ¹CT, ³CT, and ³LE states were calculated by single-point calculations via dihedral angle scan using the geometries of the respective states. The SOC constants were calculated within the ORCA program package,²³ using ZORA relativistic contraction of the TZVP basis set.

For each rotational isomer, the rate constants of ISC and rISC via ¹CT → ³CT, ¹CT → ³LE and ³CT → ¹CT, ³LE → ¹CT transitions were calculated using the Marcus–Hush equation

$$k = \frac{V^2}{\hbar} \sqrt{\frac{\pi}{k_B T \lambda}} \exp \left[-\frac{(\Delta E_{ST} + \lambda)^2}{4k_B T \lambda} \right] \quad (1)$$

where k is a rate constant, V is the SOC constant, λ is the sum of internal and external (λ_{solv}) reorganization energies for the respective transition, ΔE_{ST} is an energy gap between ¹CT and the respective triplet state, k_B is the Boltzmann constant, \hbar is the reduced Planck's constant, and T is the temperature (298.15 K). For detailed procedures and examples of calculations, see the Supporting Information.

RESULTS AND DISCUSSION

Figure 1 shows the emission spectra and decays, respectively, of DMAC-TRZ in various liquid solutions. Strong positive solvatochromism evidenced energy decrease of the ¹CT state with the increase of medium polarity. Taking into account the 440 nm onset of ³LE phosphorescence measured in frozen methylcyclohexane solution,¹⁶ the ΔE_{CT-3LE} values in these experiments varied from +0.1 eV in hexane to −0.4 eV in acetone. In further discussion, to analyze the medium effect and avoid fluctuations of composition of solvent mixtures

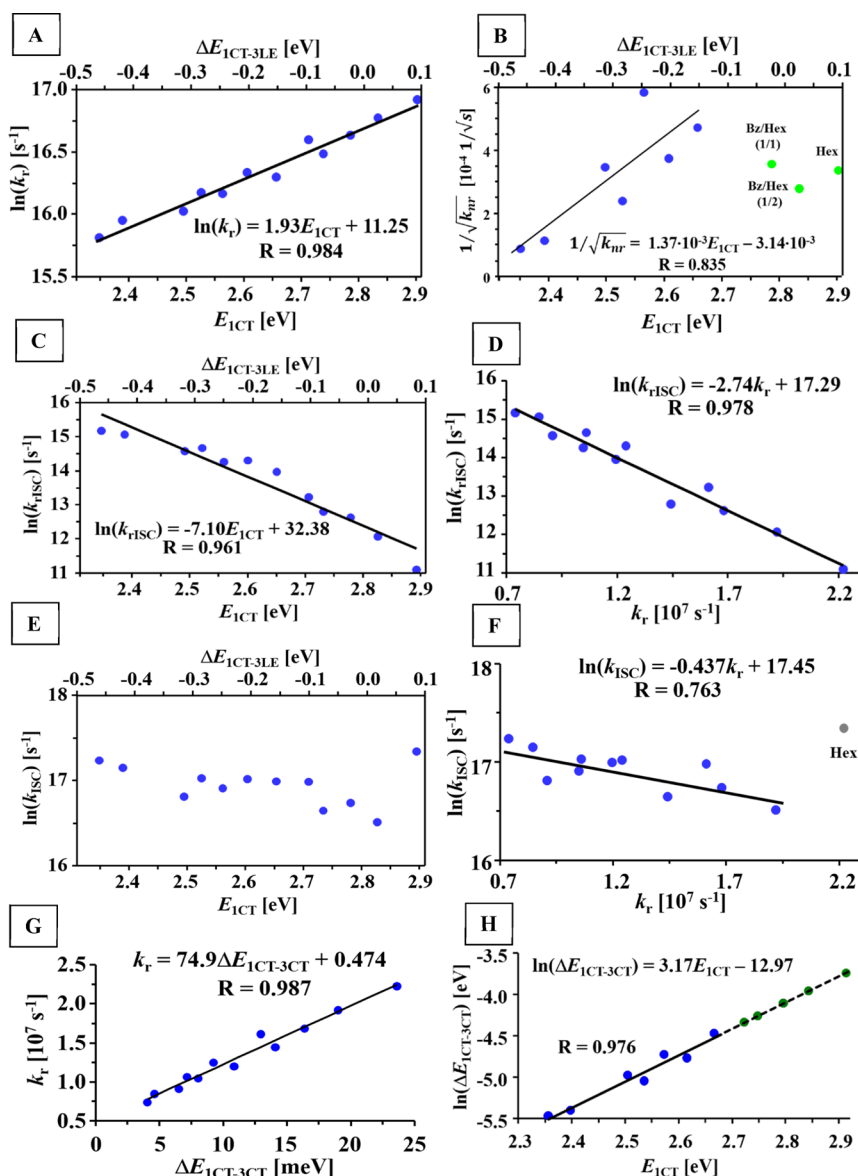


Figure 2. Dependencies of experimental rate constants of radiative (A) and nonradiative (B) deactivation, rISC (C) and ISC (E) on the energy of ^1CT state and $\Delta E_{\text{CT-}^3\text{LE}}$ energy gap. Dependencies of experimental rate constants of rISC (D) and ISC (F) on radiative rate constant. Correlation between the experimental rate constant of radiative deactivation and reconstructed $^1\text{CT-}^3\text{CT}$ energy gap (G). Logarithm of energy gap between ^1CT and ^3CT states as a function of ^1CT -state energy (H, blue points obtained using experimental k_{rISC} values, green ones calculated by extrapolation).

during the removal of oxygen, onset of fluorescence spectrum (E_{CT}) is used as an internal polarity parameter.

Rates and yields of photophysical processes are presented in Table S1 (Supporting Information). The rate constant of radiative deactivation (k_{r}) exhibited strong exponential dependence on E_{CT} (Figure 2A). The highest k_{r} value of $2.2 \times 10^7 \text{ s}^{-1}$ was obtained for an E_{CT} of 2.91 eV in non-polar hexane, while the lowest k_{r} of $7.4 \times 10^6 \text{ s}^{-1}$ was obtained for an E_{CT} of 2.36 eV in polar acetone. Such a reduction of k_{r} with the increase of polarity is well known for donor–acceptor molecular systems.²⁴ In current discussion, it should be noted that the observed dependence provides evidence that the increasing polarity and solvent-relaxation efficiency in the excited state favors more effective separation of frontier orbitals involved in the $\text{S}_1\text{-S}_0$ transition. On the one hand, this reduces oscillator strength and k_{r} . On the other hand, this

favors minimization of the exchange energy between S_1 and T_1 states of the same nature, which leads to the reduction of $\Delta E_{\text{CT-}^3\text{CT}}$ value. Within the same D–A chromophore, k_{r} can thus be referred as a measure of $\Delta E_{\text{CT-}^3\text{CT}}$. This assumption is quite important because of the lack of reliable experimental methods for the estimation of $\Delta E_{\text{CT-}^3\text{CT}}$ and ^3CT -state energy, especially in solutions and at room temperature. As will be discussed further, the determined $\Delta E_{\text{CT-}^3\text{CT}}$ in fact correlates perfectly with k_{r} .

Analysis of the emission decay profiles (Figure 1) leads to important conclusions on the polarity effect on nonradiative transitions. When polarity increases from hexane to *o*-dichlorobenzene, the time range in which emission occurs is shortened, but the intensity of the delayed component represented by the intensity of the second decay plateau is increased. This indicates the increase of rISC rate with

medium polarity. In more polar acetone and 75% acetone in hexane, the time range of emission shortens sharply, indicating strong increase of nonradiative deactivation. In terms of the determined parameters (Table S1, Supporting Information), in a low-polarity medium, the rate constant of nonradiative deactivation (k_{nr}) of 1CT state is minimal, when $\Delta E_{^1CT-^3LE}$ is close to zero. One can thus suggest that the energetic closeness of 1CT and 3LE states is important for high PLQY. In more polar solvents, lower 1CT level corresponds to faster nonradiative deactivation. Importantly, the increase of k_{nr} is the key factor decreasing PLQY in polar media but not the changes in ISC or rISC rates. In polar media, the main nonradiative deactivation channel is most likely internal conversion, the rate constant of which is proportional to $1/\Delta E_{S_1-S_0}$.^{2,25} In fact, k_{nr} shows good correlation with $1/\Delta E_{S_1-S_0}$ in polar media (Figure 2B), but not in the low-polar one, indicating different mechanisms of nonradiative deactivation probably due to slow rISC.

rISC Rate. To present further evidence of $\Delta E_{^1CT-^3CT}$ dependence on polarity, rISC is discussed prior to ISC. The value of k_{rISC} shows strong logarithmic dependence on polarity of medium, namely, $E_{^1CT}$ as a polarity parameter: the lower the $E_{^1CT}$, the higher the $\ln(k_{rISC})$ (Figure 2C). In terms of the $\Delta E_{^1CT-^3LE}$ energy gap, rISC reaches highest rate when 1CT is most separated from the 3LE state. In contrast to the three-state model, experimental data thus do not support maximal rISC rate at the point of energetic degeneracy of CT and locally excited states. When $E_{^1CT}$ decreases, the alignment of excited states changes (Figure 3): 3CT becomes the lowest triplet state and the fraction of excited molecules in the second triplet state (3LE) decreases sharply. Despite that $\Delta E_{^1CT-^3LE}$ becomes negative increasing the driving force of $^3LE \rightarrow ^1CT$ transition, decreased population of the 3LE state should result in k_{rISC} decrease, which is not the case.

Figure 3 illustrates the significance of reorganization energy $\lambda_{^1CT \leftrightarrow ^3LE}$ and driving force $\Delta E_{^1CT-^3LE}$ for the transitions between the 1CT and 3LE states of different geometries. Within the Marcus theory, the maximum rate of $^3LE \rightarrow ^1CT$ transition is not predicted for the same energy of the 1CT and 3LE states because of the additional reorganization energy involved. If rISC occurs via the $^3LE \rightarrow ^1CT$ transition, the dependence of k_{rISC} on $E_{^1CT}$ should contain two regions. First is "normal region", where $-\Delta E_{^1CT-^3LE} < \lambda_{^1CT \leftrightarrow ^3LE}$ (Figure 3, hexane and benzene). In this region, the rISC rate should increase, when $-\Delta E_{^1CT-^3LE}$ draws closer to $\lambda_{^1CT \leftrightarrow ^3LE}$ and reach maximum, when these values are equal. In the second region, "inverted region", where $-\Delta E_{^1CT-^3LE} > \lambda_{^1CT \leftrightarrow ^3LE}$, the rISC rate should decrease as the $-\Delta E_{^1CT-^3LE}$ value increases (Figure 3, *o*-dichlorobenzene). Clearly, these regions are not observed in the experimental k_{rISC} on $E_{^1CT}$ dependence.

On the other hand, the experimental rISC rate shows strong exponential dependence on k_r (Figure 2D), which as suggested above correlates with the energy gap between the CT states of different multiplicity. At this point, it is concluded that k_{rISC} is strongly dependent on $\Delta E_{^1CT-^3CT}$ but not the $\Delta E_{^1CT-^3LE}$ value.

To explain the experimental dependences, the effect of specific molecular vibrations on the electronic features of DMAC-TRZ is analyzed. As was mentioned above, in the optimal geometries with ideally orthogonal DMAC and TRZ fragments, SOCME between 3CT and 1CT states is 0.00 cm^{-1} which excludes the possibility of efficient spin-flip transition. It is however well known that at temperatures above 0 K ,

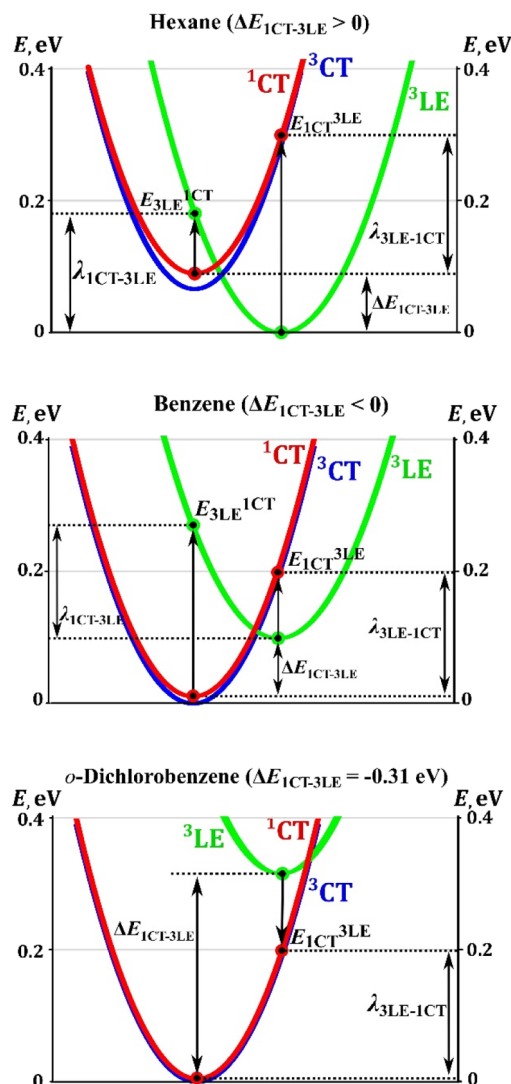


Figure 3. Potential energy curves of the lowest excited states in various media.

molecules exist in the excited vibronic states. Molecular vibrations are responsible for the violation of some selection rules such as symmetry forbidden and $n-\pi^*$ transitions.²⁶ Similarly, the transitions forbidden by the El-Sayed rule, based on the electronic nature of states, can occur due to vibrational coupling perturbations. Apparently, a theoretical model describing photophysics of TADF emitters should take into account the effect of molecular vibrations on geometry. In the first vibronic mode of DMAC-TRZ, the dihedral angle (θ) between the donor and acceptor is changing (Figure 4A). Such molecular vibrations have immense influence on electronic properties, and therefore, the model presented below is based on these vibrations.

Importantly, SOC between the 3CT and 1CT states was found to be extremely sensitive to the dihedral angle θ (Figure 4B): SOCME is zero in optimal geometry with θ of 90° , rises up to 0.05 cm^{-1} at 85° , and reaches 0.2 cm^{-1} when θ is below 65° . The discussed vibrational mode has lower energy in the 3CT state (9.84 cm^{-1}) as compared to 1CT (13.20 cm^{-1}). Consequently, the energies (Figure 4C) and molar fractions (Figure 4D) of rotational isomers are also different in the 1CT and 3CT states. In the 1CT state, rotamer energy increases by

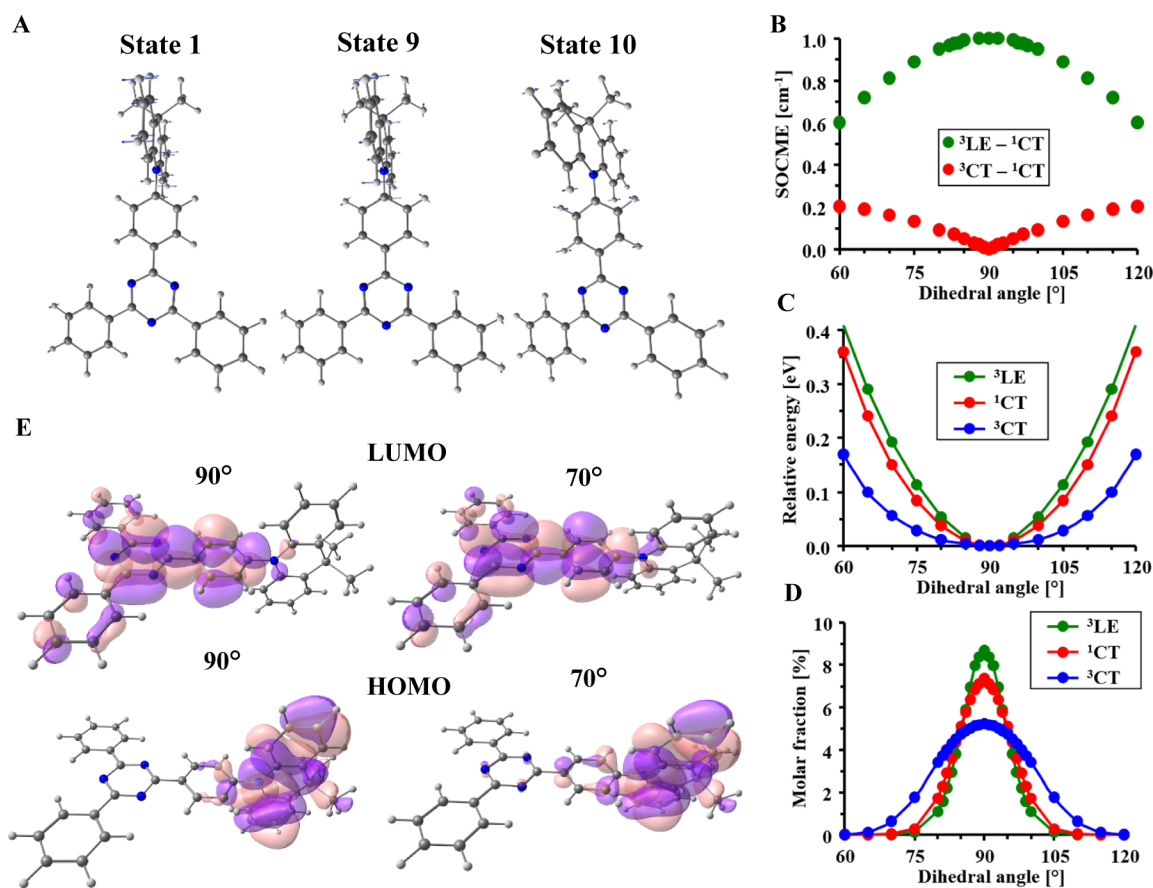


Figure 4. (A) Vectors of atomic movements in selected lowest vibrational states of the ¹CT state. (B) Dependence of SOCME between ³LE-¹CT (³LE geometry) and ³CT-¹CT (same for the ³CT and ¹CT geometries) states on the dihedral angle between donor and acceptor fragments. (C) Dependence of the relative energy of excited state on the dihedral angle. (D) Dependence of the molar fractions of rotational isomers at room temperature. (E) HOMO and LUMO calculated for various torsion angles between DMAC and TRZ fragments (contour value 0.017, ¹CT-state geometry).

0.2 eV when θ reaches 67 or 113°, while for the ³CT state, this value is 58° (122°). For this reason, mean SOCME values of 0.043 and 0.051 cm⁻¹ are obtained for the ¹CT → ³CT and ³CT → ¹CT transitions, respectively. The increase of SOC under deviation from orthogonality is explained by the increasing overlap of molecular orbitals involved in CT transitions, namely, increased contribution of the phenyl-*s*-triazine fragment in HOMO (Figure 4E).

The same analysis conducted for the ³LE → ¹CT transition in the ³LE-state geometry revealed that the SOCME value between these two states is 1.0 cm⁻¹. This value is very close to most of other organic TADF systems explained so far via the three-state model.^{5,6,10,14,15} The SOC of the ³LE → ¹CT transition in DMAC-TRZ decreases when the torsional angle θ deviates from 90° (Figure 4B). Higher energy of the discussed rotation also results in lower contribution of the rotational isomers than in the case of CT state (Figure 4D).

Prior to the theoretical prediction of rISC rate using the Marcus-Hush equation (see Methods), the effect of dihedral angle θ on $\Delta E_{\text{CT-}^3\text{CT}}$ and reorganization energy should be analyzed. Expectedly, deviation from orthogonal geometry and increase of HOMO-LUMO overlap cause the increase of $\Delta E_{\text{CT-}^3\text{CT}}$. When $\theta = 90^\circ$, TD-DFT/B3LYP calculations predict the $\Delta E_{\text{CT-}^3\text{CT}}$ value of 6.6 meV, which rises up gradually to 0.20 eV at 60° (Figure S1, Supporting Information). Within the Marcus theory, internal (structural)

and external (solvent) reorganization energies are distinguished. For the ³CT → ¹CT transition, calculations predict very low structural reorganization energy <0.5 meV, which is independent of θ within 90–65°. Due to a very similar geometry and electronic parameters of these two states, solvent reorganization energy (λ_{solv}) should also be low. One can expect that similar to $\Delta E_{\text{CT-}^3\text{CT}}$, the λ_{solv} value should increase together with the growing difference between the electronic parameters of the ³CT and ¹CT states. In further calculations, we thus assumed that the sum of reorganization energies for ³CT ↔ ¹CT transitions ($\lambda_{\text{CT-}^3\text{CT}}$) is equal to $\Delta E_{\text{CT-}^3\text{CT}}$.

The rISC rate constant calculated as a statistical sum of the rate constants of ³CT → ¹CT transition for various rotational isomers using the Marcus-Hush equation and calculated $\Delta E_{\text{CT-}^3\text{CT}}$ and SOCME values (Table S2, Supporting Information) gives a $k_{\text{CT} \rightarrow \text{CT}}$ value of $2.26 \times 10^6 \text{ s}^{-1}$. This value matches perfectly the experimental k_{rISC} value of $2.1 \times 10^6 \text{ s}^{-1}$ in *o*-dichlorobenzene. The predicted S₁-S₀ transition maximum of 611 nm is also in good correlation with the experimental emission maximum in *o*-dichlorobenzene at 570 nm.

Such a remarkable match of experimental and computational data leads to two main conclusions. First, the B3LYP calculations of D-A-type emitters correlate very well with the experiment in the medium of relatively high polarity. The most important conclusion is that the ³CT → ¹CT transition

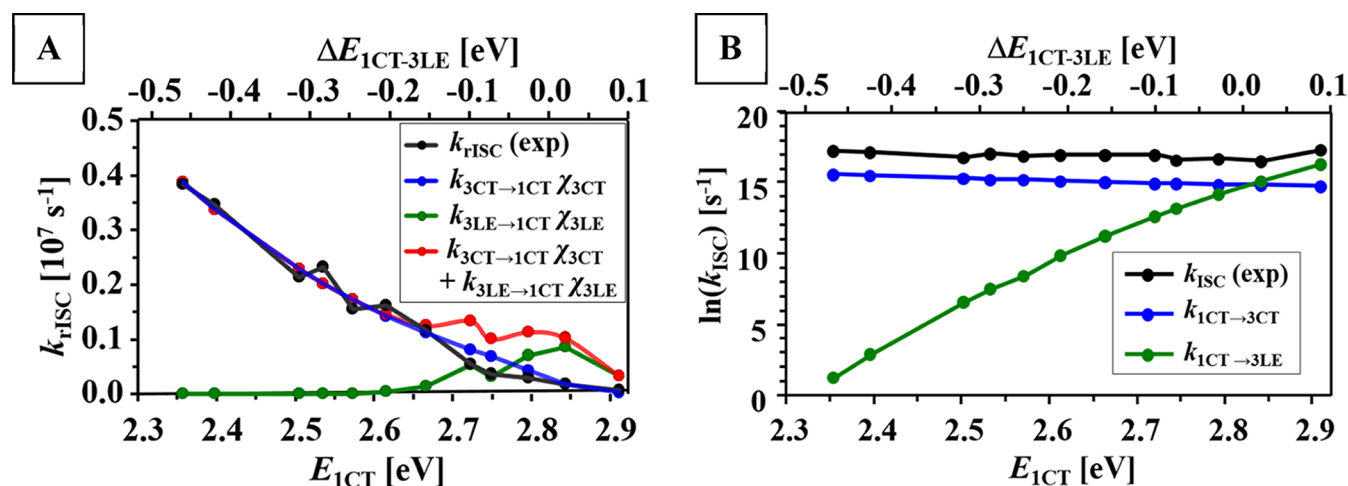


Figure 5. Comparison of calculated (Table S3) and experimental (Table S1) rates of triplet–singlet transitions (A) and singlet–triplet transitions in logarithmic scale (B) in a function of ${}^1\text{CT}$ -state energy. The rate constants of ${}^3\text{LE} \leftrightarrow {}^1\text{CT}$ transitions were calculated using $\lambda_{\text{solv}} = 0.3$ eV.

can solely afford high rISC rates due to molecular vibrations. High rate of ${}^3\text{CT} \rightarrow {}^1\text{CT}$ transition is a combination of couple of factors. First is vibrationally activated SOC between the same CT states of different multiplicities. Even though it is 10–20 times smaller than the SOC between the ${}^3\text{LE}$ and ${}^1\text{CT}$ states, the small $\Delta E_{\text{CT}-{}^3\text{CT}}$ energy gap together with almost identical geometry and thus comparably small reorganization energy enable fast ${}^3\text{CT} \rightarrow {}^1\text{CT}$ rate. As discussed further, the reorganization energy of ${}^3\text{LE} \rightarrow {}^1\text{CT}$ transition is much larger, which is a decisive factor in favor of ${}^3\text{CT} \rightarrow {}^1\text{CT}$ transition.

Similar analysis of the experimental k_{rISC} in polar media ($E_{\text{CT}} \leq 2.67$ eV) was done. Under such conditions, according to the Boltzmann distribution, the population of ${}^3\text{LE}$ state is below 0.2% and thus ${}^3\text{LE} \rightarrow {}^1\text{CT}$ transition cannot contribute considerably to rISC. The ${}^3\text{CT} \rightarrow {}^1\text{CT}$ transition is thus the only pathway of rISC and its parameters can be estimated. The $\Delta E_{\text{CT}-{}^3\text{CT}}$ values corresponding to experimental k_{rISC} according to the Marcus–Hush equation are presented in Table S1 (Supporting Information). The thus-obtained $\Delta E_{\text{CT}-{}^3\text{CT}}$ values decrease with the rise of medium polarity, which supports perfectly the conclusions drawn above based on the experimental k_{r} values (Figure 2G). The dependence of $\Delta E_{\text{CT}-{}^3\text{CT}}$ on E_{CT} is best fitted by a logarithmic function (Figure 2H). Its extrapolation afforded the $\Delta E_{\text{CT}-{}^3\text{CT}}$ values in less polar media. Consequently, the lowest energy gap of 4.2 meV is obtained for the most polar acetone solution, while the highest value of 24 meV corresponds to the hexane solution.

The $k_{\text{CT} \rightarrow \text{CT}}$ values calculated using the reconstructed dependence of $\Delta E_{\text{CT}-{}^3\text{CT}}$ on E_{CT} are compared with the experimental k_{rISC} in Figure 5A. To take into account the medium-dependent population of species in ${}^3\text{CT}$ and ${}^3\text{LE}$ states, $k_{\text{CT} \rightarrow \text{CT}}$ is multiplied by the molar fraction of molecules in the ${}^3\text{CT}$ state at 298 K (χ_{CT}).

In the media of lower polarity with $E_{\text{CT}} \geq 2.72$ eV, the molar fractions of species in the ${}^3\text{LE}$ state should be taken into account (Table S3, Supporting Information). To calculate the rate of ${}^3\text{LE} \rightarrow {}^1\text{CT}$ transition, the experimental $\Delta E_{\text{CT}-{}^3\text{LE}}$ and computationally predicted structural reorganization energies ($\lambda_{\text{LE} \rightarrow \text{CT}}^3$, 0.209–0.226 eV) for various rotational isomers were used (for detailed procedure, see the Supporting Information). The thus-obtained $k_{\text{LE} \rightarrow \text{CT}}^3$ ($\lambda_{\text{solv}} = 0.3$ eV) multiplied by the molar fraction of molecules in the ${}^3\text{LE}$ state at 298 K (χ_{LE}) are plotted in Figure 5A (for calculations using lower λ_{solv} see the

Supporting Information). According to this, the ${}^3\text{LE} \rightarrow {}^1\text{CT}$ transition should have the key contribution to rISC in the region of low polarity with E_{CT} close to 2.8 eV and $\Delta E_{\text{CT}-{}^3\text{LE}}$ close to zero. In this region, the three-state model predicts maximum rISC rate, which is well described by the dependence of calculated $k_{\text{LE} \rightarrow \text{CT}}^3$ on E_{CT} . This however completely contradicts our experimental data: k_{rISC} do not reach any maximum at $\Delta E_{\text{CT}-{}^3\text{LE}} \approx 0$. In contrast, the experimental dependence of k_{rISC} on E_{CT} is almost perfectly described by the rates of ${}^3\text{CT} \rightarrow {}^1\text{CT}$ transition, but by neither the ${}^3\text{LE} \rightarrow {}^1\text{CT}$ one nor the sum of rates of these two transitions even in the low-polarity region (Figure 5A). Therefore, the data presented above unambiguously prove the decisive role of ${}^3\text{CT} \rightarrow {}^1\text{CT}$ transition, but not the ${}^3\text{LE} \rightarrow {}^1\text{CT}$ one in the rISC process in DMAC-TRZ.

ISC Rate. ISC is another important process representing forward transformation of singlet S_1 state to the triplet ones. ISC and rISC are closely connected; thus, any theoretical model which explains rISC but fails to describe correctly ISC cannot be regarded as satisfactory.

The experimental ISC rate shows complex dependence on the ${}^1\text{CT}$ -state energy (Figure 2E). In hexane ($E_{\text{CT}} = 2.91$ eV), an ISC rate constant (k_{ISC}) value of $3.4 \times 10^7 \text{ s}^{-1}$ is the highest, but it decreases sharply to $1.5 \times 10^7 \text{ s}^{-1}$ in the benzene–hexane (1:2, v/v) mixture, where the E_{CT} value is 2.84 eV. A further decrease of E_{CT} causes gradual increase of k_{ISC} up to $3.1 \times 10^7 \text{ s}^{-1}$ in acetone. According to the alignment of excited states, the decrease of E_{CT} in polar media makes the ${}^1\text{CT} \rightarrow {}^3\text{LE}$ transition endothermic (Figure 3). Under such a distancing of ${}^1\text{CT}$ and ${}^3\text{LE}$ states, if the ${}^1\text{CT} \rightarrow {}^3\text{LE}$ transition was the main pathway of ISC, a sharp decrease of k_{ISC} with the $\Delta E_{\text{CT}-{}^3\text{LE}}$ value would be observed, which is not the case.

In contrast, k_{ISC} grows exponentially with the decrease of k_{r} (Figure 2F), regarded as a measure of reduction of the ${}^1\text{CT}-{}^3\text{CT}$ energy gap. These findings provide evidence that when the ${}^1\text{CT}$ and ${}^3\text{CT}$ states have lower energy than the ${}^3\text{LE}$ one, ISC occurs mainly via the ${}^1\text{CT} \rightarrow {}^3\text{CT}$ channel in the nanosecond regime, even though it is forbidden by the El Sayed’s rules.

Similar to rISC, two mechanisms of ISC in DMAC-TRZ can be suggested: ${}^1\text{CT} \rightarrow {}^3\text{LE}$ and ${}^1\text{CT} \rightarrow {}^3\text{CT}$ transitions. In hexane, the ${}^1\text{CT} \rightarrow {}^3\text{LE}$ transition rate calculated using the Marcus–Hush equation is close to experimental k_{ISC} . However,

in more polar media, $k_{CT \rightarrow ^3LE}$ decreases sharply (Figure 5B) due to the increasing negative value of $\Delta E_{CT \rightarrow ^3LE}^1$ and thus growing endothermicity of this process. For example, in acetone and *o*-dichlorobenzene, $k_{CT \rightarrow ^3LE}$ does not exceed 3 and $1 \times 10^3 \text{ s}^{-1}$, respectively, and thus, its contribution to ISC is negligible. On the other hand, the rate constant of $^1CT \rightarrow ^3CT$ transition calculated as a statistical sum of $k_{CT \rightarrow ^3CT}^1$ of various rotational isomers correlates well with the experimental k_{ISC} in all the investigated media except for hexane: $k_{CT \rightarrow ^3CT}^1$ increases with the decrease of E_{CT}^1 (Figure 5B). The reason of such a dependence is the above-mentioned decrease of $\Delta E_{CT \rightarrow ^3CT}^1$ with growing medium polarity. Therefore, in almost all experimental conditions, ISC proceeds via the $^1CT \rightarrow ^3CT$ transition. Only in non-polar hexane, where the CT states are the least stabilized and $\Delta E_{CT \rightarrow ^3CT}^1$ reaches maximum, both pathways are realized and the $^1CT \rightarrow ^3LE$ transition contributes noticeably to ISC.

In spite of perfect prediction of $k_{ISC} - E_{CT}^1$ dependence, the calculated $k_{CT \rightarrow ^3CT}^1$ values are ca. 4–5 times lower than the experimental ones. Apparently, real SOCME values of the $^1CT \rightarrow ^3CT$ transition are higher. Similarly, the radiative deactivation rate calculated as the statistical sum of various rotational isomers (described in detail in the Supporting Information) is 4.2 times underestimated as compared to the experimental value in *o*-dichlorobenzene (Table S4, Supporting Information). It should be noticed that the discussed approach is a simplified model based on the first-mode vibrations. Even though these vibrations have the key influence on the electronic properties of the CT states due to the change of dihedral angle θ between donor and acceptor planes, some other vibrations of higher energies also reduce the separation of HOMO and LUMO (Figure 4A). For example, vibrations of the ninth vibronic state also change θ , and in the tenth state, the planarity of the donor is disrupted. These vibrations lead to further increase of SOC as well as oscillator strength and k_r . More correct description of each TADF emitter should take into account the influence of all vibrations characteristic for each compound on the CT state. It should be noticed that, in general, understanding of vibrational enhancement of SOC cannot be simplified to the conformational changes. We, however, believe that the simplified approach presented here can be successfully used for design and semiquantitative unified description of rates of ISC, rISC, and radiative deactivation of a large number of D–A-type emitters with an orthogonal structure.

Connection with Other Investigations. The analysis of experimental reports on other emitters proves that within similar molecular systems, the highest rISC and/or external quantum efficiency (EQE) is achieved when the CT states are most stabilized and thus, as concluded above, $\Delta E_{CT \rightarrow ^3CT}^1$ is minimized. This can be achieved in two ways. First is the change of medium or the host matrix. The reported experiments generally provide evidence that higher polarity favors faster rISC and, in the absence of nonradiative deactivation, higher photo- and electroluminescence efficiency. As an example, 2,7-bis(9,9-dimethyl-acridin-10-yl)-9,9-dimethylthioxanthene-*S,S*-dioxide (DDMA-TXO2) exhibited faster rISC in the DPEPO host than in Zeonex films,²⁷ OLED devices containing tBUCzDCNPy emitter showed more than 3 times higher EQE when the DPEPO host was used instead of less polar mCP,²⁸ as well as TTAZ and TXAZ emitters dispersed in the DPEPO host instead of the less polar medium, the mixture of mCP and TSPO1 (1:1) hosts.²⁹

Almost all previous theoretical models were developed on the basis of experimental photophysical data in the media of low polarity such as OLED hosts (mCP, CBP, DPEPO, etc.) or polymer matrixes such as Zeonex, polystyrene, and PMMA. Within such media, the variation of E_{CT}^1 of a selected emitter usually does not exceed 0.15 eV, which is too small to study a case with large $\Delta E_{CT \rightarrow ^3LE}^1$. Another important remark: in TADF emitters bearing conjugated fragments such as phenothiazine, phenoxazine, phenyl-*s*-triazine, phenylpyrimidine, phenazine, benzophenone, naphthalimide, and so forth, as well as some carbazole derivatives and similar aromatic heterocycles, the 3LE energies are relatively low and, in non-polar medium, represent the T_1 states. Numerous TADF emitters can serve as examples: PTZ-DBTO2,³⁰ DPTZ-DPTO2,³¹ and their derivatives based on which the three-state model was mainly developed, numerous *s*-triazine derivatives,^{14–16,29,32} DBT-BZ-DMAC,³³ NAI,³⁴ various indolo[3,2-*b*]indole derivatives,³⁵ POZ-DBPHZ,³⁶ and so on. When polarity increases, the CT states of such emitters are getting energetically closer to 3LE , but simultaneously, the energy difference between 1CT and 3CT states also decreases, which most likely plays the key role in TADF.

The second way to change the CT-state energies is chemical modification. According to the literature reports, within derivatives bearing similar donor and acceptor fragments, better TADF parameters are observed in the emitters with higher donor/acceptor strength. For example, in toluene, DMAC-TRZ¹⁶ bearing strong *s*-triazine acceptor shows higher rISC rate ($7 \times 10^5 \text{ s}^{-1}$) as compared to its weaker 2-pyrimidine (no TADF) and 4-pyrimidine analogues ($6 \times 10^4 \text{ s}^{-1}$).³⁷ In the DPEPO host, despite a larger absolute $\Delta E_{CT \rightarrow ^3LE}^1$ value, CT states of DMAC-TRZ are more stabilized and afford EQE_{max} of 25%, in contrast to the pyrimidine analogues not exceeding 8% and 12%, respectively. Similarly, the change of spiroacridine donor to a weaker phenazasiline one in combination with the same aryl-1,3,5-triazine acceptors led to destabilization of CT states, slower TADF, and lower EQE.²⁹

The only one known example of a molecular emitter with an extremely small $\Delta E_{CT \rightarrow ^3CT}^1$ value of $< 2 \text{ meV}$ and a large $\Delta E_{CT \rightarrow ^3LE}^1$ value of 0.2 eV serves as an excellent proof for the key importance of energetic closeness of 3CT and 1CT (compound 2, ref 38). Taking into account the very low $\Delta E_{CT \rightarrow ^3CT}^1$ value emphasized by authors, the experimental evidence of very fast ISC and rISC exceeding the rate of radiative deactivation supports the vibrationally enhanced $^3CT \leftrightarrow ^1CT$ SOC model presented here.

As concluded above, one of the factors of efficient $^3CT \leftrightarrow ^1CT$ transformation is the vibrationally enhanced SOC with an average value of 0.05 cm^{-1} . In one of the pioneering works, the phenomenon of hyperfine coupling between the 1CT and 3CT states was suggested as a main reason explaining fast population of T_1 state in TADF emitters in time-resolved EPR experiment.³⁹ According to this model, SOCME due to hyperfine interaction can however reach a maximum of 0.2 cm^{-1} , when $\Delta E_{CT \rightarrow ^3CT}^1$ is below 0.051–0.025 meV (0.4 – 0.2 cm^{-1}). This can be valid for radical pairs; however, in almost all known molecular TADF emitters, the $\Delta E_{CT \rightarrow ^3CT}^1$ value is hundred times higher. A conclusion on negligible impact of hyperfine coupling on the TADF photophysics was also made previously on the basis of theoretical modeling.⁵

Finally, the vibronically assisted ISC model was applied for the 2CzPN and 4CzIPN emitters to explain the electron spin resonance (ESP) experiments.⁴⁰ It should be mentioned that

donor and acceptor in these emitters are not completely orthogonal, which provides HOMO/LUMO overlap, differences in the S_1 and T_1 states' nature, and thus non-zero SOC with large ΔE_{ST} already in the optimal geometry.⁴¹ However, the ESP results consistent with the vibronically assisted ISC model indicate that molecular vibrations play the key role in facilitating direct ISC and rISC via the $S_1 \leftrightarrow T_1$ in such compounds. Therefore, the model presented here should be valid not only for D–A emitters with orthogonal structure and well-separated frontier molecular orbitals but also for other kinds of CT TADF emitters with appropriate ΔE_{ST} values.

In DMAC-TRZ, substantial differences in geometries and dipole moments of 1CT and 3LE states lead to large internal and external reorganization energies for the $^1CT \leftrightarrow ^3LE$ transitions. To summarize the key numerical data for DMAC-TRZ, the calculated internal reorganization energies $\lambda_{CT \rightarrow ^3LE}^1$ and $\lambda_{^3LE \rightarrow ^1CT}^1$ are 179.6 meV and 208.8, respectively, which are more than 350 times higher than the internal $\lambda_{CT \rightarrow ^3CT}^1$ value of 0.5 meV. The analysis of solvatochromic effect on the photophysical parameters revealed that the $^1CT \leftrightarrow ^3LE$ transition with large reorganization energy do not explain the experimental growth of rISC and ISC rates with the polarity of medium. In various media from hexane to acetone solutions, the $\Delta E_{CT \rightarrow ^3LE}^1$ values estimated experimentally changed in the large range from +94 to –460 meV, whereas the $\Delta E_{CT \rightarrow ^3CT}^1$ values changed from 24 to 4.2 meV. The corresponding TD-DFT calculated values were 559 and 6.6 meV, respectively. In contrast to the $^1CT \leftrightarrow ^3LE$ transitions, the $^1CT \leftrightarrow ^3CT$ ones perfectly explained the experimental dependencies due to much smaller reorganization energy and energy gap as well as vibrationally enhanced SOC.

In D–A emitters, the role of 3LE state in spin-flip processes should thus be carefully analyzed using both $\Delta E_{CT \rightarrow ^3LE}^1$ and $\lambda_{CT \rightarrow ^3LE}^1$ values, namely, how the change of latter values correlate with the experimental rate constants. In our opinion, the evidence of fast ISC and rISC between the 1CT and 3CT states presented here significantly change the current understanding of TADF photophysics. Previous interpretation of the photophysical properties of TADF emitters based on the $\Delta E_{CT \rightarrow ^3LE}^1$ value as the key parameter and negligible rate of the $^3CT \leftrightarrow ^1CT$ transitions should be reconsidered.

CONCLUSIONS

The main conclusion of this research is that correct description of the basic photophysical parameters of TADF emitters such as rates of ISC, rISC, and radiative deactivation is not possible without taking into account molecular vibrations and deviation from the orthogonality of D–A planes. A relatively simple and illustrative model presented here brings further important consequences. The evidence of efficient interaction of the same CT states with different multiplicities changes significantly the current understanding of TADF. Photophysics of some emitters as well as molecular design principles should be revised with an accent on $\Delta E_{CT \rightarrow ^3CT}^1$.

Experimental investigations of DMAC-TRZ in solvents of large range of polarity provided evidence of the increase of rates of forward and rISC under the stabilization of CT states. Supported by the TDDFT calculations, the polarity dependence of ISC and rISC was explained by the growing efficiency of the $^1CT \leftrightarrow ^3CT$ interaction, which is forbidden in “frozen” optimal excited-state geometry but is effectively activated by molecular vibrations and accelerated in polar media due to the reduction of the 1CT – 3CT energy gap.

To describe correctly the experimental data, a theoretical model was developed, which treats photophysical parameters as statistical sums of respective values for selected rotational isomers existing at room temperature. Molecular vibrations changing the dihedral angle between donor and acceptor fragments were found to increase the SOC sharply between the 1CT and 3CT states of the same nature. According to the theoretical and experimental results, ISC and rISC occur through the $^3CT \leftrightarrow ^1CT$ channel exclusively. The exception is the medium of lowest polarity, hexane, where the $\Delta E_{CT \rightarrow ^3CT}^1$ value is the highest one and the ISC rate is abnormally high, indicating some influence of the 3LE state.

The main factors enabling effective $^1CT \leftrightarrow ^3CT$ transitions are the vibrationally enhanced SOC, very small energy gap, and comparably small reorganization energy due to similar geometries in the 1CT and 3CT states. In contrast, much larger reorganization energy $\lambda_{CT \rightarrow ^3LE}^1$, growing $|\Delta E_{CT \rightarrow ^3LE}^1|$ value, and decreasing population of the 3LE state result in negligible contribution of $^3LE \leftrightarrow ^1CT$ transition rate in media more polar than hexane.

Further development of high-precision theoretical TADF model at a given temperature should take into account numerous molecular vibrations and their impact on the electronic properties of lowest excited states. Moreover, special attention should be given to the effects of viscosity of medium on molecular vibrations, especially in the case of amorphous emitting layers in optoelectronic devices.

ASSOCIATED CONTENT

Supporting Information

The Supporting Information is available free of charge at <https://pubs.acs.org/doi/10.1021/acs.jpcc.0c10605>.

Experimental photophysical parameters and detailed procedure of their determination, results of DFT calculations, detailed procedures, and examples of calculations of ISC, rISC, and k_r within the developed model (PDF)

AUTHOR INFORMATION

Corresponding Author

Illia E. Serdiuk – Faculty of Mathematics, Physics and Informatics, University of Gdańsk, 80-308 Gdańsk, Poland; orcid.org/0000-0002-4563-0773; Phone: +48 58 523 22 44; Email: illia.serdiuk@ug.edu.pl

Authors

Michał Mońka – Faculty of Mathematics, Physics and Informatics, University of Gdańsk, 80-308 Gdańsk, Poland
Karol Kozakiewicz – Faculty of Chemistry, University of Gdańsk, 80-308 Gdańsk, Poland
Beata Liberek – Faculty of Chemistry, University of Gdańsk, 80-308 Gdańsk, Poland
Piotr Bojarski – Faculty of Mathematics, Physics and Informatics, University of Gdańsk, 80-308 Gdańsk, Poland
Soo Young Park – Center for Supramolecular Optoelectronic Materials, Department of Materials Science and Engineering, Seoul National University, 151-744 Seoul, Republic of Korea; orcid.org/0000-0002-2272-8524

Complete contact information is available at: <https://pubs.acs.org/doi/10.1021/acs.jpcc.0c10605>

Notes

The authors declare no competing financial interest.

ACKNOWLEDGMENTS

I.E.S. is grateful to the Polish Ministry of Science and Higher Education for financial support within the Mobility Plus project no. 1637/MOB/V/2017/0. Quantum chemical calculations were performed on the computers of the Wrocław Centre for Networking and Supercomputing (WCSS), Poland. S.Y.P. gratefully acknowledges the financial support from Samsung Display Co., Ltd.

REFERENCES

- (1) Uoyama, H.; Goushi, K.; Shizu, K.; Nomura, H.; Adachi, C. Highly Efficient Organic Light-Emitting Diodes from Delayed Fluorescence. *Nature* **2012**, *492*, 234–240.
- (2) Nakanotani, H.; Higuchi, T.; Furukawa, T.; Masui, K.; Morimoto, K.; Numata, M.; Tanaka, H.; Sagara, Y.; Yasuda, T.; Adachi, C. High-Efficiency Organic Light-Emitting Diodes with Fluorescent Emitters. *Nat. Commun.* **2014**, *5*, 4016.
- (3) Dias, F. B.; Bourdakos, K. N.; Jankus, V.; Moss, K. C.; Kamtekar, K. T.; Bhalla, V.; Santos, J.; Bryce, M. R.; Monkman, A. P. Triplet Harvesting with 100% Efficiency by way of Thermally Activated Delayed Fluorescence in Charge Transfer OLED Emitters. *Adv. Mater.* **2013**, *25*, 3707–3714.
- (4) Noda, H.; Chen, X.-K.; Nakanotani, H.; Hosokai, T.; Miyajima, M.; Notsuka, N.; Kashima, Y.; Brédas, J.-L.; Adachi, C. Critical Role of Intermediate Electronic States for Spin-Flip Processes in Charge-Transfer-Type Organic Molecules with Multiple Donors and Acceptors. *Nat. Mater.* **2019**, *18*, 1084–1090.
- (5) Gibson, J.; Monkman, A. P.; Penfold, T. J. The Importance of Vibronic Coupling for Efficient Reverse Intersystem Crossing in Thermally Activated Delayed Fluorescence Molecules. *ChemPhysChem* **2016**, *17*, 2956–2961.
- (6) Samanta, P. K.; Kim, D.; Coropceanu, V.; Brédas, J.-L. Up-Conversion Intersystem Crossing Rates in Organic Emitters for Thermally Activated Delayed Fluorescence: Impact of the Nature of Singlet vs Triplet Excited States. *J. Am. Chem. Soc.* **2017**, *139*, 4042–4051.
- (7) Ward, J. S.; Nobuyasu, R. S.; Batsanov, A. S.; Data, P.; Monkman, A. P.; Dias, F. B.; Bryce, M. R. The Interplay of Thermally Activated Delayed Fluorescence (TADF) and Room Temperature Organic Phosphorescence in Sterically-Constrained Donor–Acceptor Charge-Transfer Molecules. *Chem. Commun.* **2016**, *52*, 2612–2615.
- (8) Zeng, W.; Gong, S.; Zhong, C.; Yang, C. Prediction of Oscillator Strength and Transition Dipole Moments with the Nuclear Ensemble Approach for Thermally Activated Delayed Fluorescence Emitters. *J. Phys. Chem. C* **2019**, *123*, 10081–10086.
- (9) Stavrou, K.; Franca, L. G.; Monkman, A. P. Photophysics of TADF Guest–Host Systems: Introducing the Idea of Hosting Potential. *ACS Appl. Electron. Mater.* **2020**, *2*, 2868–2881.
- (10) Kim, I.; Jeon, S. O.; Jeong, D.; Choi, H.; Son, W.-J.; Kim, D.; Rhee, Y. M.; Lee, H. S. Spin–Vibronic Model for Quantitative Prediction of Reverse Intersystem Crossing Rate in Thermally Activated Delayed Fluorescence Systems. *J. Chem. Theory Comput.* **2020**, *16*, 621–632.
- (11) Di, D.; Romanov, A. S.; Yang, L.; Richter, J. M.; Rivett, J. P. H.; Jones, S.; Thomas, T. H.; Abdi Jalebi, M.; Friend, R. H.; Linnolahti, M.; et al. High-Performance Light-Emitting Diodes Based on Carbene-Metal-Amides. *Science* **2017**, *356*, 159–163.
- (12) Föllner, J.; Marian, C. M. Rotationally Assisted Spin-State Inversion in Carbene–Metal–Amides Is an Artifact. *Phys. Chem. Lett.* **2017**, *8*, 5643–5647.
- (13) Feng, J.; Reponen, A. P. M.; Romanov, A. S.; Linnolahti, M.; Bochmann, M.; Greenham, N. C.; Penfold, T.; Credgington, D. Influence of Heavy Atom Effect on the Photophysics of Coinage Metal Carbene-Metal-Amide Emitters. *Adv. Funct. Mater.* **2021**, *31*, 2005438.
- (14) Cui, L.-S.; Gillett, A. J.; Zhang, S.-F.; Ye, H.; Liu, Y.; Chen, X.-K.; Lin, Z.-S.; Evans, E. W.; Myers, W. K.; Ronson, T. K.; et al. Fast Spin-Flip Enables Efficient and Stable Organic Electroluminescence From Charge-Transfer States. *Nat. Photon.* **2020**, *14*, 636–642.
- (15) Wada, Y.; Nakagawa, H.; Matsumoto, S.; Wakisaka, Y.; Kaji, H. Organic Light Emitters Exhibiting Very Fast Reverse Intersystem Crossing. *Nat. Photon.* **2020**, *14*, 643–649.
- (16) Serdiuk, I. E.; Ryoo, C. H.; Kozakiewicz, K.; Mońka, M.; Liberek, B.; Park, S. Y. Twisted Acceptors in the Design of Deep-Blue TADF Emitters: Crucial Role of the Excited-State Relaxation on the Photophysics of Methyl Substituted *s*-Triphenyltriazine Derivatives. *J. Mater. Chem. C* **2020**, *8*, 6052–6062.
- (17) Meech, S. R.; Phillips, D. Photophysics of Some Common Fluorescence Standards. *J. Photochem.* **1983**, *23*, 193–217.
- (18) Dias, F. B.; Penfold, T. J.; Monkman, A. P. Photophysics of Thermally Activated Delayed Fluorescence Molecules. *Methods Appl. Fluoresc.* **2017**, *5*, 012001.
- (19) Tao, Y.; Yuan, K.; Chen, T.; Xu, P.; Li, H.; Chen, R.; Zheng, C.; Zhang, L.; Huang, W. Thermally Activated Delayed Fluorescence Materials Towards the Breakthrough of Organoelectronics. *Adv. Mater.* **2014**, *26*, 7931–7958.
- (20) Labanowski, J. K. *Density Functional Methods in Chemistry*; Andzelm, J. W., Ed.; Springer-Verlag: New York, 1991.
- (21) Frisch, M. J.; Trucks, G. W.; Schlegel, H. B.; Scuseria, G. E.; Robb, M. A.; Cheeseman, J. R.; Scalmani, G.; Barone, V.; Petersson, G. A.; Nakatsuji, H.; et al. *Gaussian 16*, Revision C.01; Gaussian, Inc.: Wallingford, CT, 2016.
- (22) Becke, A. D. A New Mixing of Hartree–Fock and Local Density-Functional Theories. *J. Chem. Phys.* **1993**, *98*, 1372–1377.
- (23) Neese, F. The ORCA Program System. *Wiley Interdiscip. Rev.: Comput. Mol. Sci.* **2012**, *2*, 73–78.
- (24) Kapturkiewicz, A.; Herbich, J.; Karpiuk, J.; Nowacki, J. Intramolecular Radiative and Radiationless Charge Recombination Processes in Donor–Acceptor Carbazole Derivatives. *J. Phys. Chem. A* **1997**, *101*, 2332–2344.
- (25) Shizu, K.; Noda, H.; Tanaka, H.; Taneda, M.; Uejima, M.; Sato, T.; Tanaka, K.; Kaji, H.; Adachi, C. Highly Efficient Blue Electroluminescence Using Delayed-Fluorescence Emitters with Large Overlap Density between Luminescent and Ground States. *J. Phys. Chem. C* **2015**, *119*, 26283–26289.
- (26) Valeur, B. *Molecular Fluorescence: Principles and Applications*; Wiley-VCH Verlag GmbH, 2001; p 30.
- (27) Dos Santos, P. L.; Ward, J. S.; Bryce, M. R.; Monkman, A. P. Using Guest–Host Interactions To Optimize the Efficiency of TADF OLEDs. *J. Phys. Chem. Lett.* **2016**, *7*, 3341–3346.
- (28) Gan, L.; Gao, K.; Cai, X.; Chen, D.; Su, S.-J. Achieving Efficient Triplet Exciton Utilization with Large ΔE_{ST} and Nonobvious Delayed Fluorescence by Adjusting Excited State Energy Levels. *J. Phys. Chem. Lett.* **2018**, *9*, 4725–4731.
- (29) Woo, S.-J.; Kim, Y.; Kwon, S.-K.; Kim, Y.-H.; Kim, J.-J. Phenazasiline/Spiroacridine Donor Combined with Methyl-Substituted Linkers for Efficient Deep Blue Thermally Activated Delayed Fluorescence Emitters. *ACS Appl. Mater. Interfaces* **2019**, *11*, 7199–7207.
- (30) Nobuyasu, R. S.; Ren, Z.; Griffiths, G. C.; Batsanov, A. S.; Data, P.; Yan, S.; Monkman, A. P.; Bryce, M. R.; Dias, F. B. Rational Design of TADF Polymers Using a Donor–Acceptor Monomer with Enhanced TADF Efficiency Induced by the Energy Alignment of Charge Transfer and Local Triplet Excited States. *Adv. Optical Mater.* **2016**, *4*, 597–607.
- (31) Etherington, M. K.; Gibson, J.; Higginbotham, H. F.; Penfold, T. J.; Monkman, A. P. Revealing the Spin–Vibronic Coupling Mechanism of Thermally Activated Delayed Fluorescence. *Nat. Commun.* **2016**, *7*, 13680.
- (32) Tanaka, H.; Shizu, K.; Miyazaki, H.; Adachi, C. Efficient Green Thermally Activated Delayed Fluorescence (TADF) from a Phenoxazinetriphenyltriazine (PXZ-TRZ) Derivative. *Chem. Commun.* **2012**, *48*, 11392–11394.

(33) Guo, J.; Li, X.-L.; Nie, H.; Luo, W.; Gan, S.; Hu, S.; Hu, R.; Qin, A.; Zhao, Z.; Su, S.-J.; et al. Achieving High-Performance Nondoped OLEDs with Extremely Small Efficiency Roll-Off by Combining Aggregation-Induced Emission and Thermally Activated Delayed Fluorescence. *Adv. Funct. Mater.* **2017**, *27*, 1606458.

(34) Zeng, W.; Zhou, T.; Ning, W.; Zhong, C.; He, J.; Gong, S.; Xie, G.; Yang, C. Realizing 22.5% External Quantum Efficiency for Solution-Processed Thermally Activated Delayed-Fluorescence OLEDs with Red Emission at 622 nm via a Synergistic Strategy of Molecular Engineering and Host Selection. *Adv. Mater.* **2019**, *31*, No. e1901404.

(35) Ryoo, C. H.; Cho, I.; Han, J.; Yang, J.-h.; Kwon, J. E.; Kim, S.; Jeong, H.; Lee, C.; Park, S. Y. Structure–Property Correlation in Luminescent Indolo[3,2-b]indole (IDID) Derivatives: Unraveling the Mechanism of High Efficiency Thermally Activated Delayed Fluorescence (TADF). *ACS Appl. Mater. Interfaces* **2017**, *9*, 41413–41420.

(36) Data, P.; Pander, P.; Okazaki, M.; Takeda, Y.; Minakata, S.; Monkman, A. P. Dibenzo[a,j]phenazine-Cored Donor-Acceptor-Donor Compounds as Green-to-Red/NIR Thermally Activated Delayed Fluorescence Organic Light Emitters. *Angew. Chem., Int. Ed.* **2016**, *55*, 5739–5744.

(37) Ganesan, P.; Ranganathan, R.; Chi, Y.; Liu, X.-K.; Lee, C.-S.; Liu, S.-H.; Lee, G.-H.; Lin, T.-C.; Chen, Y.-T.; Chou, P.-T. Functional Pyrimidine-Based Thermally Activated Delay Fluorescence Emitters: Photophysics, Mechanochromism, and Fabrication of Organic Light-Emitting Diodes. *Chem. Eur. J.* **2017**, *23*, 2858–2866.

(38) Yersin, H.; Mataranga-Popa, L.; Czerwieniec, R.; Dovbii, Y. Design of a New Mechanism beyond Thermally Activated Delayed Fluorescence toward Fourth Generation Organic Light Emitting Diodes. *Chem. Mater.* **2019**, *31*, 6110–6116.

(39) Ogiwara, T.; Wakikawa, Y.; Ikoma, T. Mechanism of Intersystem Crossing of Thermally Activated Delayed Fluorescence Molecules. *J. Phys. Chem. A* **2015**, *119*, 3415–3418.

(40) Evans, E. W.; Olivier, Y.; Puttisong, Y.; Myers, W. K.; Hele, T. J. H.; Menke, S. M.; Thomas, T. H.; Credgington, D.; Beljonne, D.; Friend, R. H.; et al. Vibrationally Assisted Intersystem Crossing in Benchmark Thermally Activated Delayed Fluorescence Molecules. *J. Phys. Chem. Lett.* **2018**, *9*, 4053–4058.

(41) Hosokai, T.; Matsuzaki, H.; Nakanotani, H.; Tokumaru, K.; Tsutsui, T.; Furube, A.; Nasu, K.; Nomura, H.; Yahiro, M.; Adachi, C. Evidence and Mechanism of Efficient Thermally Activated Delayed Fluorescence Promoted by Delocalized Excited States. *Sci. Adv.* **2017**, *3*, No. e1603282.